5. ACTIVE GALAXIES

Matthew Baring – Lecture Notes for ASTR 360, Spring 2025

1 Global Energetics of Active Galaxies

• Active galaxies were discovered largely since WWII, both with developments in optical astronomy and the advent of radio astronomy. Key signatures of active galaxies include that they are typically much more luminous than normal galaxies, with $L \sim 10^{42} - 10^{47}\,$erg/sec. This is generally interpreted to imply that *their energy source is not nuclear*.

∗ In stellar nucleosynthesis, since main sequence stars are typically 5 orders of magnitude larger than their Schwarzschild radii, the efficiency of tapping their gravitational potential is of order 10^{-5} of their rest mass $\Rightarrow$ **Kelvin-Helmholtz** $t_{\rm KH}$ timescales exceed the Hubble time $t_{\rm H}$.

The efficiency nuclear energy production is at best 0.7% (for He production in the *pp* chain; talk about the nuclear binding energy curve). With an estimate $E_{\rm nucl} \sim 0.007 m_p c^2 N_p$, one finds

$$10^{47}\,{\rm erg/sec} \;\equiv\; 5.6\times 10^{-8} M_\odot c^2/{\rm sec} \;\sim\; 2.4\times 10^{10} M_\odot c^2/t_{\rm H} \quad . \qquad (1)$$

Hence core masses of $10^9 M_\odot$ are insufficient to sustain the luminosity over a Hubble time via nuclear means alone.

• In contrast, active galaxies possess compact cores that are designated **active galactic nuclei**, and these tap much stronger gravitational potentials.

∗ Gravity can, in principal, be 100 times more efficient, being sampled via **accretion** of matter onto a general relativistic **supermassive black hole** (SMBH) that serves as the **central engine** or powerhouse.

2 Seyferts

• **Seyfert galaxies** are spirals with extremely bright cores that almost render them star-like in appearance — overexposed photos must be taken to discern their spiral structure. They were discovered in 1943 by Carl Seyfert. **C & O, pp. 1085–7**

∗ Key signatures include a non-thermal continuum in the visible, X-rays and even soft gamma-rays. They tend not to be strong radio sources.

∗ *emission lines* in the spectrum, resembling (hot) HII regions more than stars that exhibit absorption features.

• **Type I Seyferts** possess broad permitted lines like H_β , indicating Doppler velocities $v_{\rm D} \sim 5,000 - 10,000\,{\rm km/sec}$. This high velocity gas ($\sim c/30$) suggests the action of a relativistic environment (=SMBH?).

∗ they also exhibit much narrower **forbidden lines** such as OII, OIII, NII, SII etc. with $v_{\rm D} \sim 300\,{\rm km/sec}$. Forbidden lines require low gas densities, typically $\lesssim 10^8\,{\rm cm}^{-3}$ in order to be present $\Rightarrow \sim 50 M_\odot$ in NLR gas.

In **Type II Seyferts**, only the narrower lines are present.

Plot: Narrow and Broad Line Profiles in Seyferts

• The standard explanation is that distinct regions **BLR** and **NLR** for the production of broad and narrow emission lines exist, with the BLR being more proximate to the SMBH. The are both proximate to a central gas **accretion disk** that flares out to a **dusty torus**. **C & O, pp. 1116–9**

Plot: AGN Geometry with BLR and NLR

• Much dust and gas is believed to be expelled from Seyfert nuclei, and this may enshroud the nucleus itself at radii $\lesssim 1\,{\rm light\ year}$. The dust is inferred to be at a temperature $T \lesssim 2000\,{\rm K}$ from the observed IR bump in the Seyfert continuum spectrum. It is believed that much dust resides in a **torus** extending outwards from the inner accretion disk that emits continuum thermal radiation in the UV that is often referred to as the **big blue bump**.

Narrow and Broad Line Profiles

Goodrich (1995, ApJ **440**, 141)

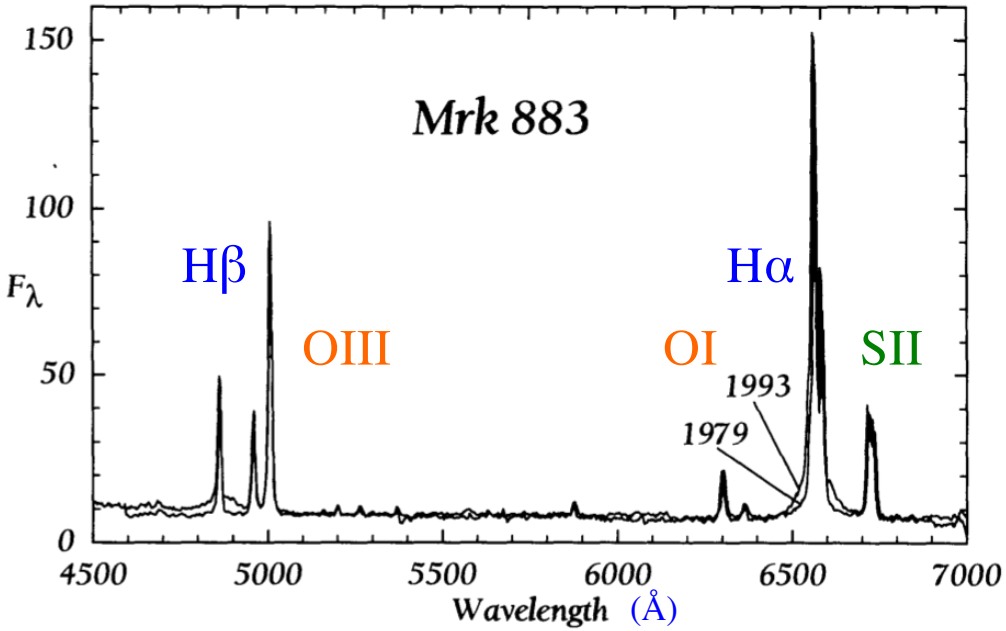

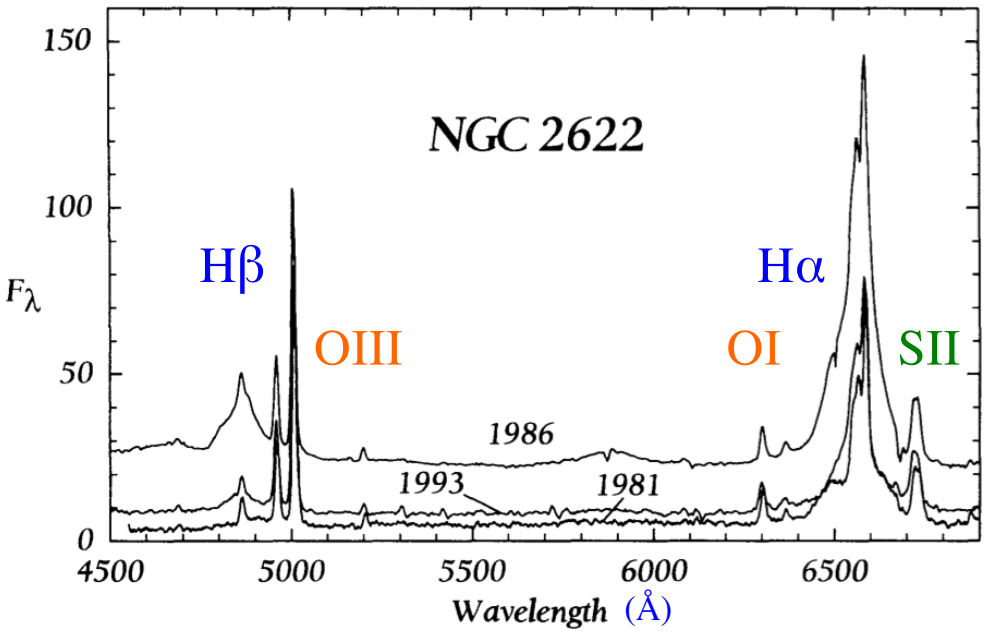

- Optical/NIR emission line profiles for two Seyfert galaxies demonstrating time variability.
- *Left*: Mrk 883 exhibits narrow OIII lines around λ=4959Å and 5007Å, broad Balmer Hα around 6548Å and Hβ around 4860Å. *Right*: NGC 2622 has a much broader Hα feature but still narrow OIII lines. OI lines (6300Å & 6364Å) and SII lines (6717Å & 6731Å; blended) are visible in both Seyfert spectra. From Goodrich (1995, ApJ **440**, 141). Higher resolution spectroscopy resolves SII doublets (e.g. Osterbrock & Dahari 1983, ApJ **273**, 478).

Generic AGN Geometry

Blazars

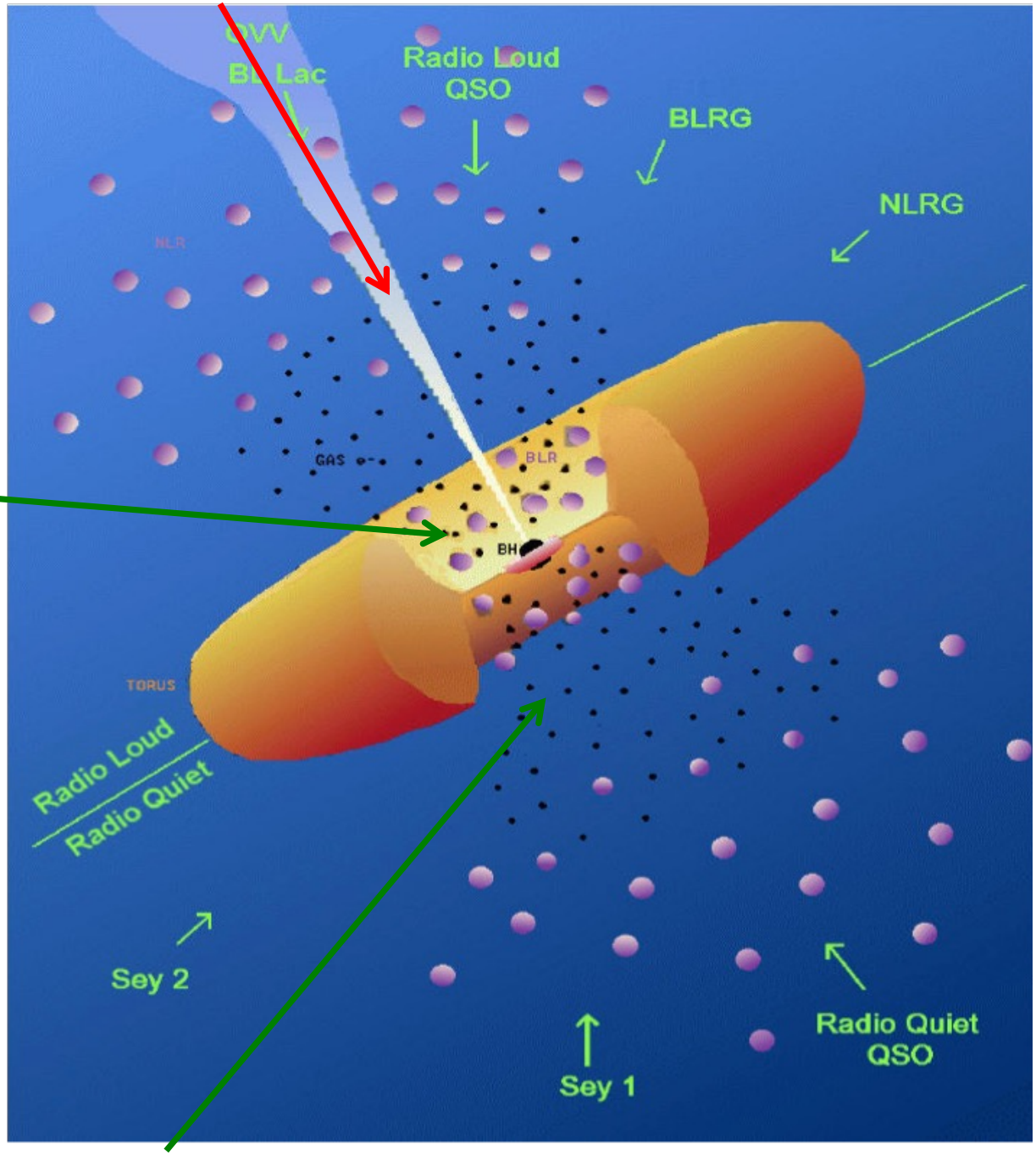

Broad line region

Narrow line region

- Schematic of geometry of active galactic nuclei. Adapted from Urry & Padovani (1995, PASP, **107**, 803).

• Time variability on scale of weeks suggests a size scale of $R_{\rm BLR} \lesssim 10^{16}\,{\rm cm}$. The NLR does not have profound variability on timescales shorter than a year, and so must be at least $10^2 \to 10^3$ times larger. Interpreting the BLR as bounding the radius of the SMBH suggests $R_{\rm BH} = 2GM/c^2 \sim 3 \times 10^{13}\,{\rm cm}$ $\Rightarrow M \sim 10^8 M_\odot$!

• Similar variability bounds can be obtained by measuring time delays τ between variations in the brightness of the continuum and the emission lines. This technique is known as **reverberation mapping**. Then $r \sim c\tau$ provides an estimate of the physical size of the emission region, and $\sigma \sim (\Delta v) \sim c\,\Delta\lambda/\lambda$ is the velocity width or dispersion of an emission line.

These then combine for a *virial estimate* of the mass of the central black hole:

$$M_{\rm BH} \sim \frac{r\,(\Delta v)^2}{G} \sim \frac{c\tau\,\sigma^2}{G} \sim 10^7 - 10^9 M_\odot \quad . \tag{2}$$

This reverberation mapping technique establishes the typical range of masses for SMBHs, and therefore indicates that active galaxies radiate at sizeable fractions of their **Eddington luminosity**.

Plot: Reverberation Mapping AGN Black Hole Mass Determination

• If the radiation pressure force exceeds the gravitational one, which is GM/r^2 per unit mass for a central black hole of mass M, then the plasma that emits the observed radiation cannot stably exist at a radius r, and would be expelled out to infinity. The balance between these two forces establishes an upper bound to the radiation luminosity:

$$L < L_{\rm Edd} \equiv \frac{4\pi GMm_p c}{\sigma_{\rm T}} = 1.25 \times 10^{38}\,\frac{M}{M_\odot}\,{\rm erg/sec}\,. \tag{3}$$

known as the **Eddington limit**. $\sigma_{\rm T}$ is the Thomson cross section. Active galaxies like Seyferts and quasars generally satisfy this fundamental bound.

• Seyferts exhibit **strong Fe K-spectral lines** in their X-ray spectra, superposed on a **Compton reflection** continuum. These lines are gravitationally redshifted from their natural 6.4 keV energy and Doppler broadened. The shape of this line distortion can be used to measure the general relativistic **spin angular momentum** parameter a/M for the black hole.

Plot: Black Hole Rotation Diagnostics from Fe Lines

Reverberation Mapping and SMBH Masses

$M = v^2 \tau c / G$

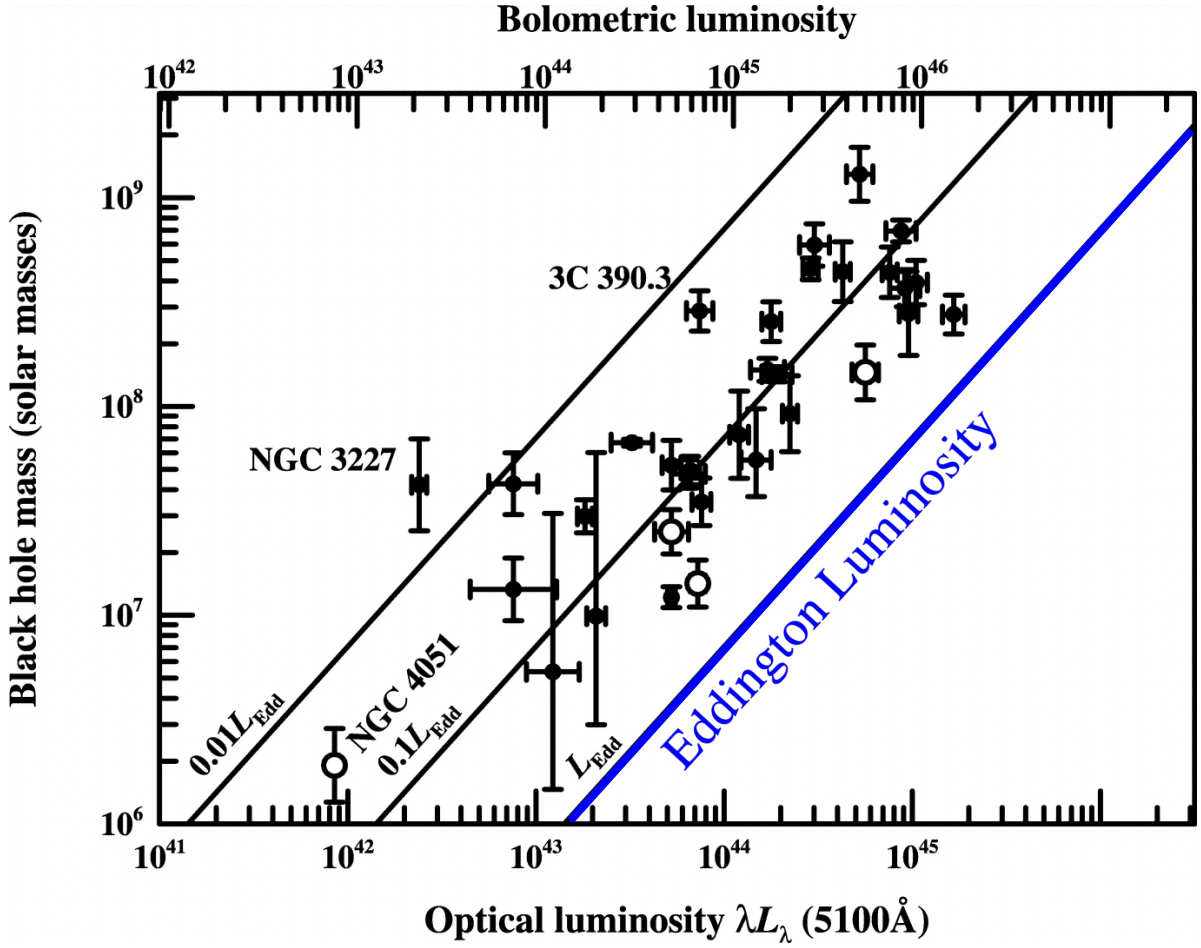

- Black hole mass vs. luminosity for 35 reverberation-mapped AGNs. The scale on the lower x-axis is log λL_λ in units of ergs s^{-1}. The upper x-axis shows the bolometric luminosity assuming that $L_{bol} \sim 10\lambda L_\lambda$. The diagonal lines show the Eddington limit L_{Edd}, $0.1L_{Edd}$, and $0.01L_{Edd}$. Fig. 16 from Peterson et al. (2004, ApJ, **613**, 682). See also the AGN black hole mass database http://www.astro.gsu.edu/AGNmass (Bentz & Katz, PASP 2015, **127**, 67).

Black Hole Rotation Diagnostics using Fe Lines from Accretion Disks

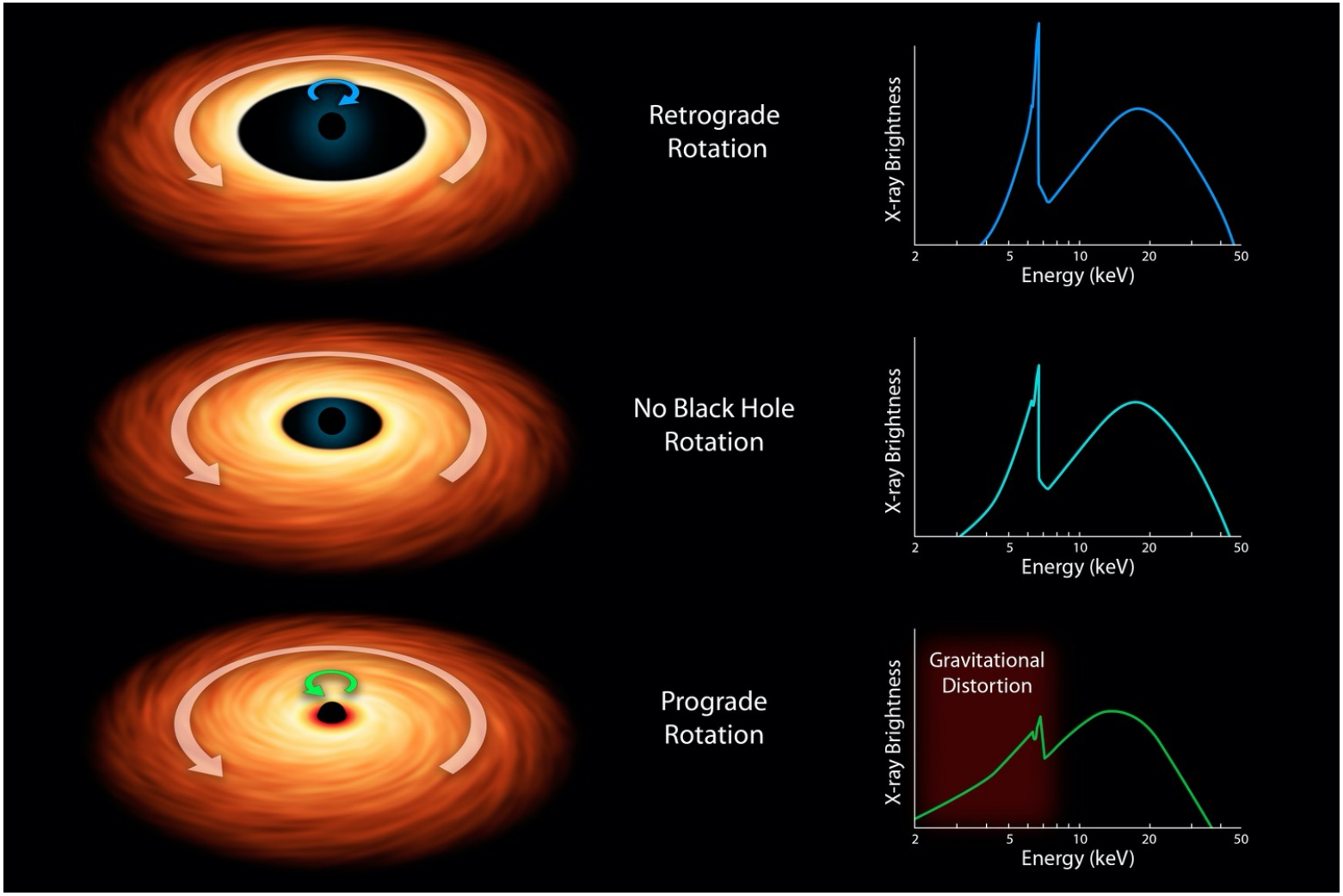

- Slide courtesy of NuStar Collaboration – for sample implementation using NGC1365 galaxy, see Risaliti, G., et al. 2013, Nature, **494, 449.**

3 Radio Galaxies

• Radio galaxies are on average more distant than Seyferts, and are obviously marked by luminous radio emission with $L_{\rm rad} \gtrsim 10^{40}\,{\rm erg/sec}$. There are two key types: **compact radio galaxies**, whose radio extent is contained within the optical angular extent; and **extended radio sources**, whose radio extent is usually beyond 50 kpc and can reach around 1 Mpc.

C & O, pp. 1090–5

∗ Radio galaxies are nearly all ellipticals, e.g. M87.

Doubles (e.g. M87, Cen A) have huge **lobes**, luminous cores and jets often with radio luminosities $L_{\rm jet} \gtrsim 10^{41}\,{\rm erg/sec}$.

Plot: 6cm Image of Radio Galaxy Cygnus A

The nuclear origin of jets is obvious, as is the fact that lobes denote zones of dynamic dissipation of the outflow.

• The radio emission is *non-thermal and highly-polarized*, even in the jet, implying it is **synchrotron radiation**. This mechanism results from relativistic charges (electrons) orbiting in magnetic fields possessing considerable order in their spatial structure. Non-relativistic electrons generate coherent cyclotron radiation, and the incoherent sum of many harmonics produced by relativistic charges is synchrotron radiation.

Plot: Synchrotron Radiation and its Spectrum

∗ The radiation is inherently non-thermal, implying the existence of a source of acceleration of electrons. The radio index (for a spectrum $\varepsilon_\gamma^{-\alpha}$) is typically $\alpha \sim 0.6$ while the optical index is $\alpha \sim 1.7$. The break in the IR [*sketch this*] implies a change in the electron distribution, and maybe due to *cessation of cooling* at low γ_e.

• Magnetic fields in radio jets can be estimated by invoking **equipartition**, i.e. the field energy density is comparable to that of the radiation:

$$\frac{B^2}{8\pi} \sim U_\gamma \equiv \frac{L_\gamma}{4\pi R^2 c} \sim \frac{10^{45}}{4\pi (10^{14})^2\,(3\times 10^{10})} \quad \Rightarrow \quad B \sim 3\times 10^3\ {\rm G} \quad (4)$$

in a region of (variability) size $R \sim 10^{14}\,{\rm cm}$.

Cygnus A: a Powerful Radio Galaxy

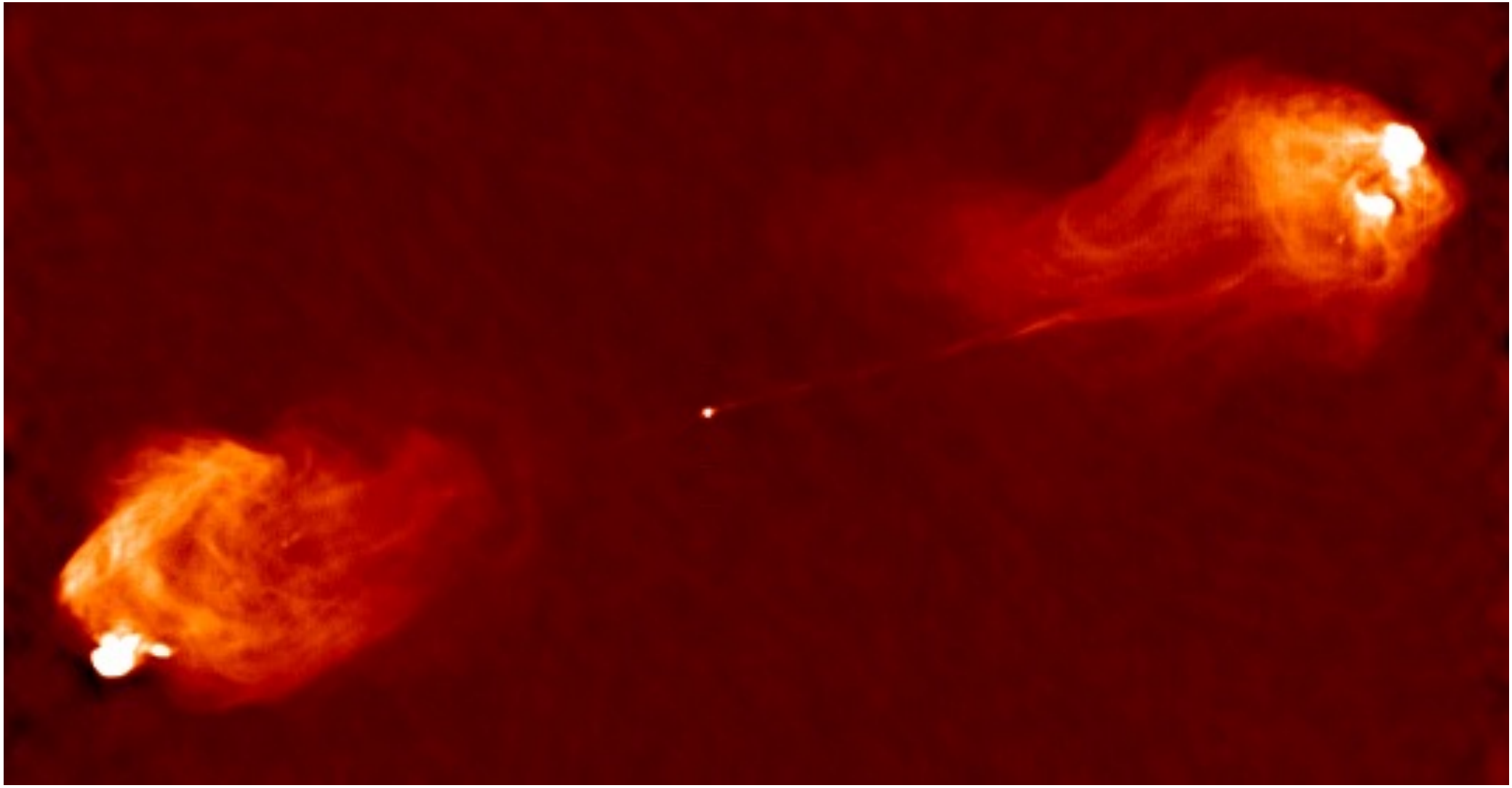

VLA image at 6cm of the most famous of double-lobed radio sources.

Classical Synchrotron Spectrum and Polarization

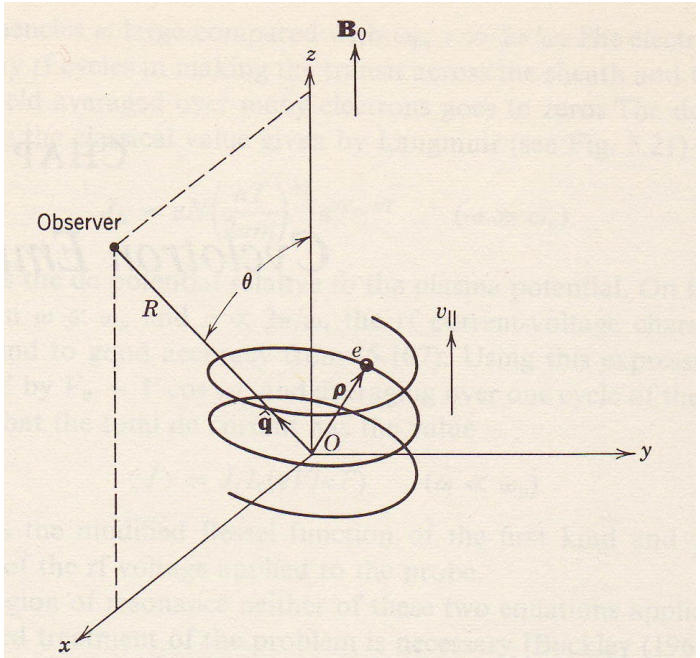

Fig. 6.1 Vector diagram for an electron in helical motion in a uniform magnetic field.

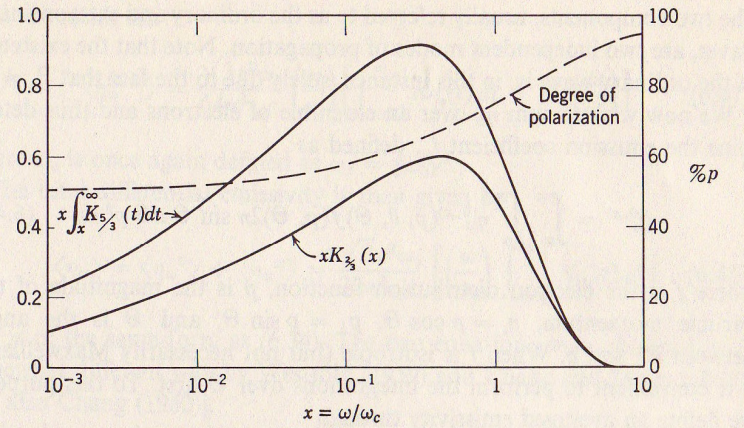

Fig. 6.7 Functions associated with the emission spectrum of a highly relativistic electron. [See Eqs. (6.34), (6.47), and (6.49).] The plots are obtained from tabulated values of Westfold (1959).

Bekefi (1966)

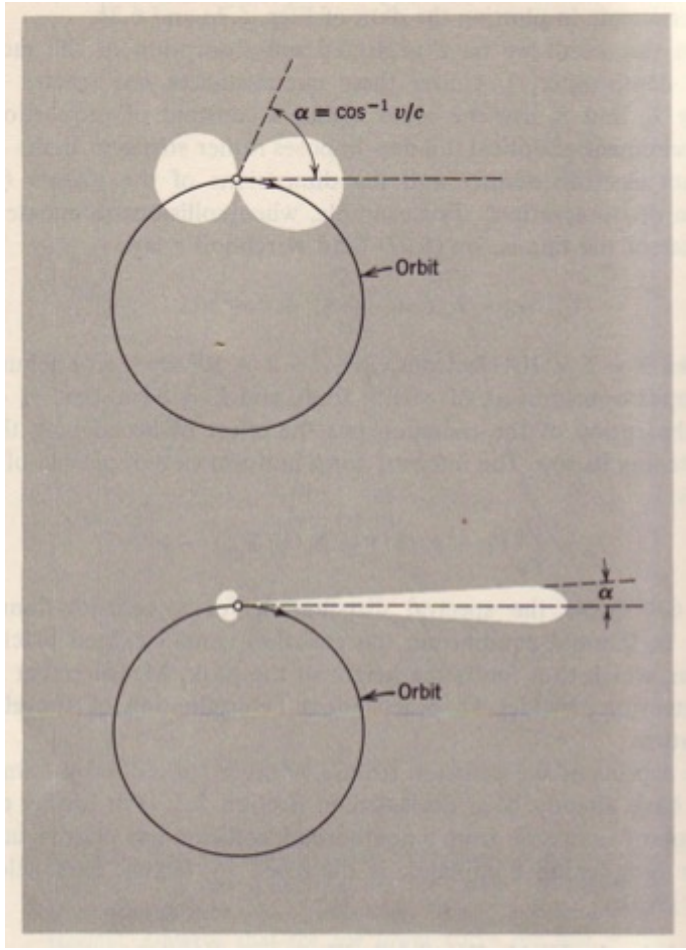

- Monoenergetic electrons: spectrum is broad (left) and radiation is beamed (right);
- Non-thermal electrons yield broad, quasi-power-law synchrotron spectrum of strong polarization;

• Jets are highly-structured, containing blobs or **knots** that are less than 1 light year across and that (in the radio) can vary on timescales of 3-10 years.

Plot: VLBI Images of Radio Galaxy NGC 6251

∗ Each knot displays similar broad-band spectra, suggesting local generation of the relativistic electron population. This inference is reinforced by images in X rays closely resembling those in radio.

Plot: Radio and X ray images of M87 and PKS 1127-145 Jets

• Fine-scale mapping of structures in radio jets is achieved through **very-long baseline array interferometry** (VLBI/VLBA). The diameter $d_\oplus$ of the Earth establishes the baseline, and the phase difference $\delta \lesssim 1$ of signals at wavelength λ from two points separated by angle θ yields

$$\theta \sim \frac{\lambda}{d} \quad \Rightarrow \quad \theta_{\rm arcsec} \sim 42\,\frac{\lambda_{21\rm cm}}{d_{\rm km}} \quad , \tag{5}$$

for the angular resolution by a telescope separation d. To resolve small angular scales θ, one requires large baselines $d_\oplus$ (i.e., VLBI) at a fixed wavelength. The ultimate radio interferometer is the Event Horizon Telescope (EHT) in the *mm* band (shorter λ than GHz band), which has obtained the spectacular images of SMBH environs in M87 and the Milky Way.

Plot: Principal of Interferometry

• The knotty structure is attributed to MHD instabilities in dynamic outflows, with **entrainment** of external material as the jet propagates outward. Radio images on the kpc scale indicate that the jet structure may consist of a fast moving central column or **spine** of low plasma density, surrounded by a slower-moving (but still relativistic), denser **sheath** that captures the entrainment. Shocks may develop at the spine-sheath interface, and may seed acceleration of electrons to relativistic energies.

Plot: Relativistic Hydrodynamic Jet Simulations

∗ The magnetic field morphology in jets is not precisely known, but may be quasi-helical as opposed to sheet-like in character. Radio polarimetry images on the kpc scale suggest that the field alignment differs between the spine and sheath, being more radial along the spine.

High Resolution Radio View of a Jet

- Radio intensity contours for the NGC 6251 jet at different wavelengths, demonstrating both multi-scale and knotty structure.
- Lower resolution data (top) are from the Westerbork (WSRT) facility in the Netherlands. Higher resolution views are from the Very Large Array (VLA) in NM, and the enlarged view of the core (bottom) was obtained using multi-facility Very-Long Baseline Interferometry (VLBI).
- Fig. 2 from classic review of Bridle & Perley (1984, Ann. Rev. Astron. Astrophys. **22**, 319).

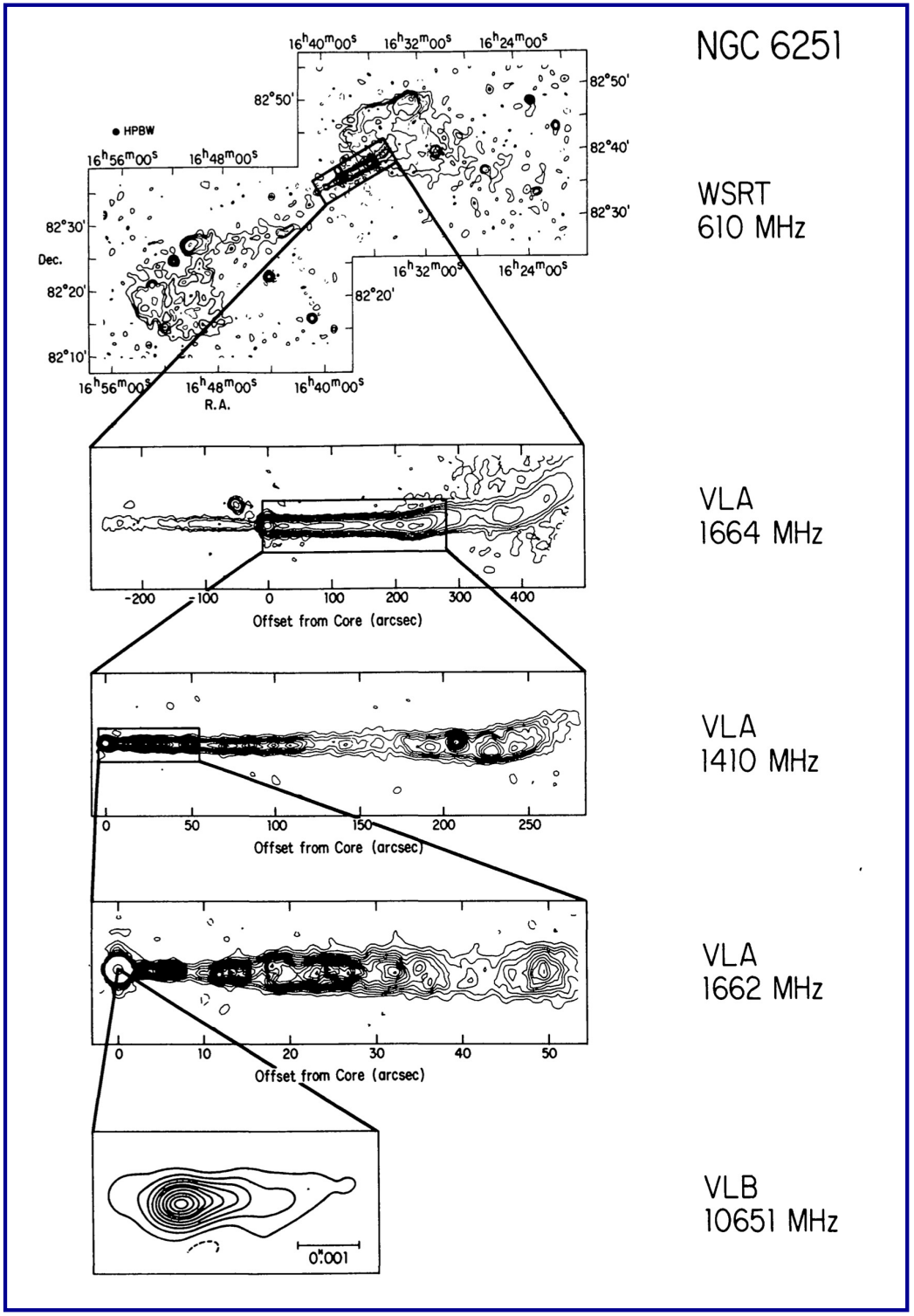

Supermassive Black Hole Jet Morphology

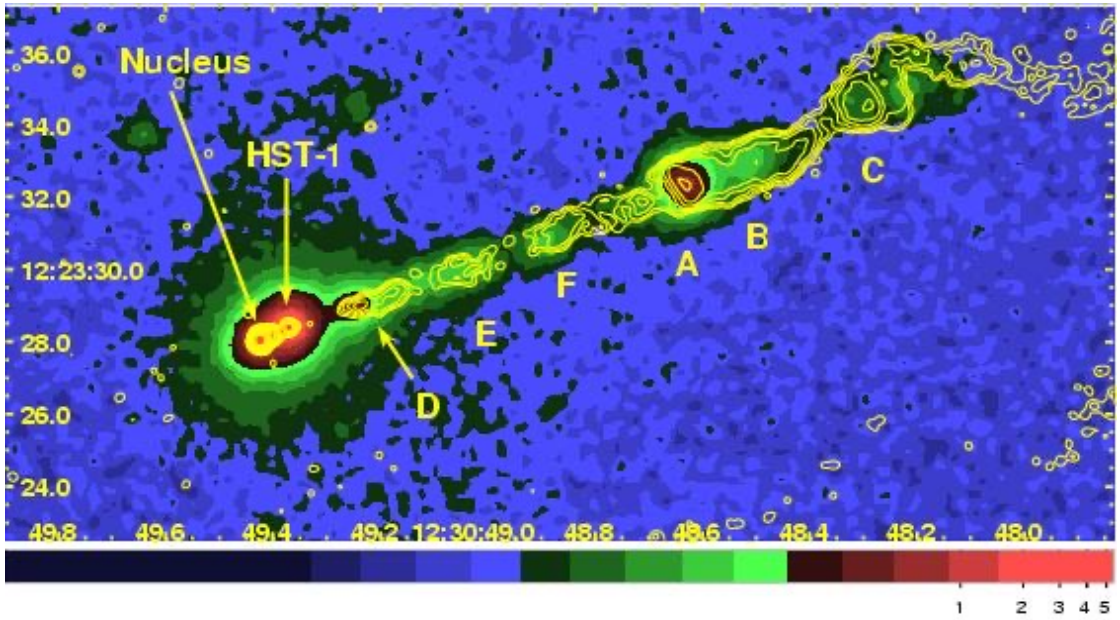

- *Above*: M87 jet (z=0.0043) as viewed by *Chandra* (0.2-6 keV), with VLA 8 GHz radio contours superimposed.
- *Right*: Combined *Chandra* X-ray and VLA 8 GHz radio data for the PKS 1127-145 jet (z=1.18).
- Figures from extragalactic jet review by Harris & Krawczynski (2006, ARAA 44, 463)

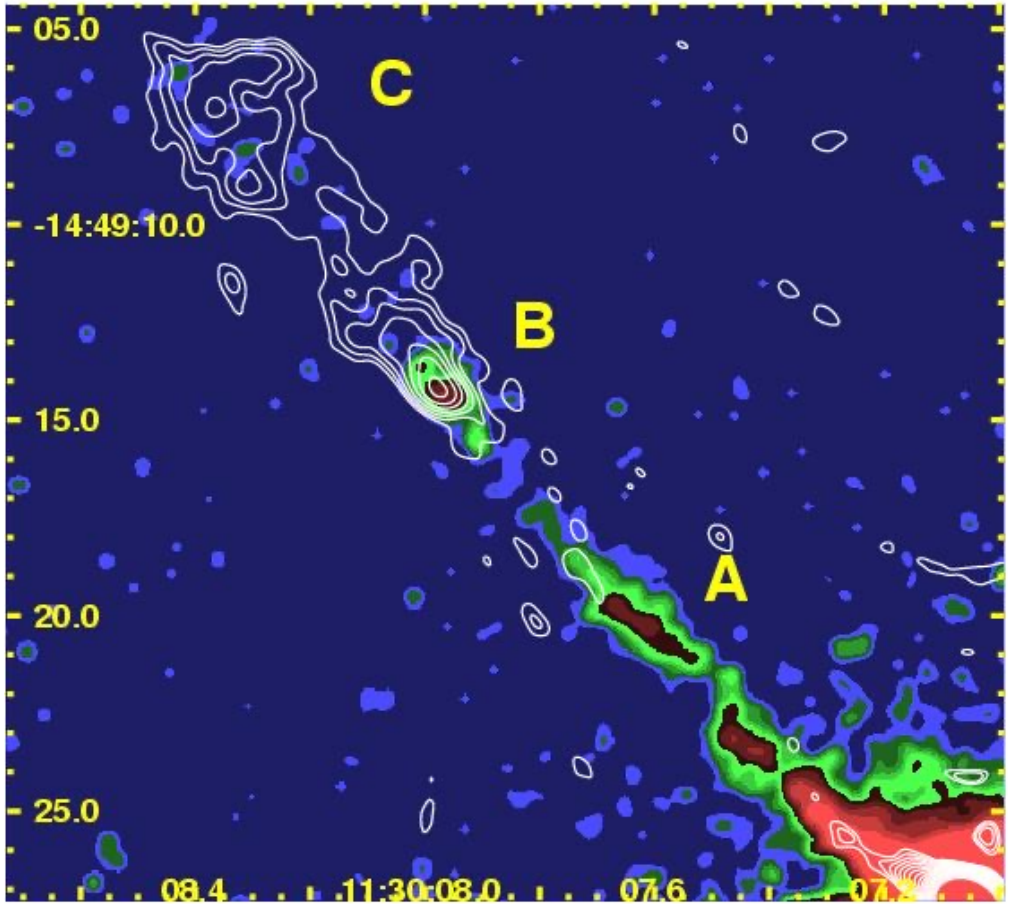

Radio Interferometry Geometry

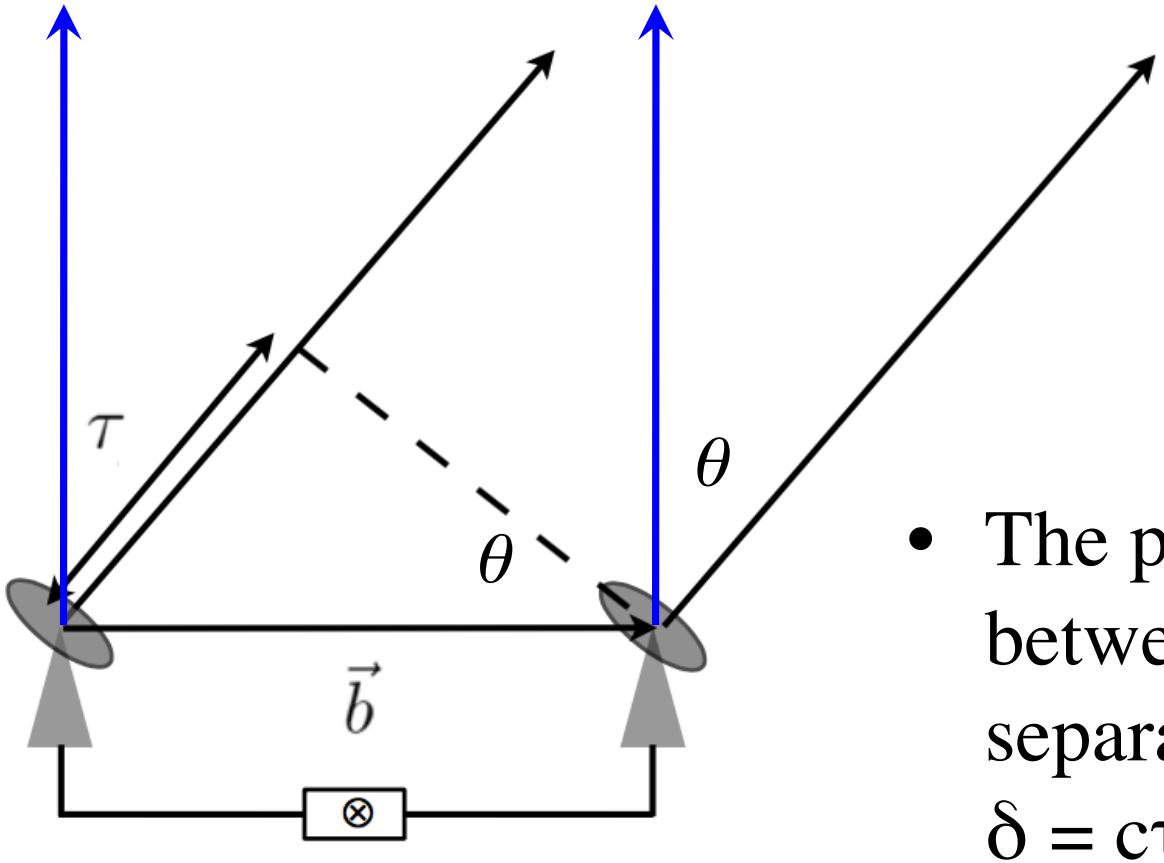

- The phase difference between signals separated by angle θ is $\delta = c\tau/\lambda \sim b\theta/\lambda$.
- Large baseline b gives resolution of small θ.

Hydrodynamics of Relativistic Jets

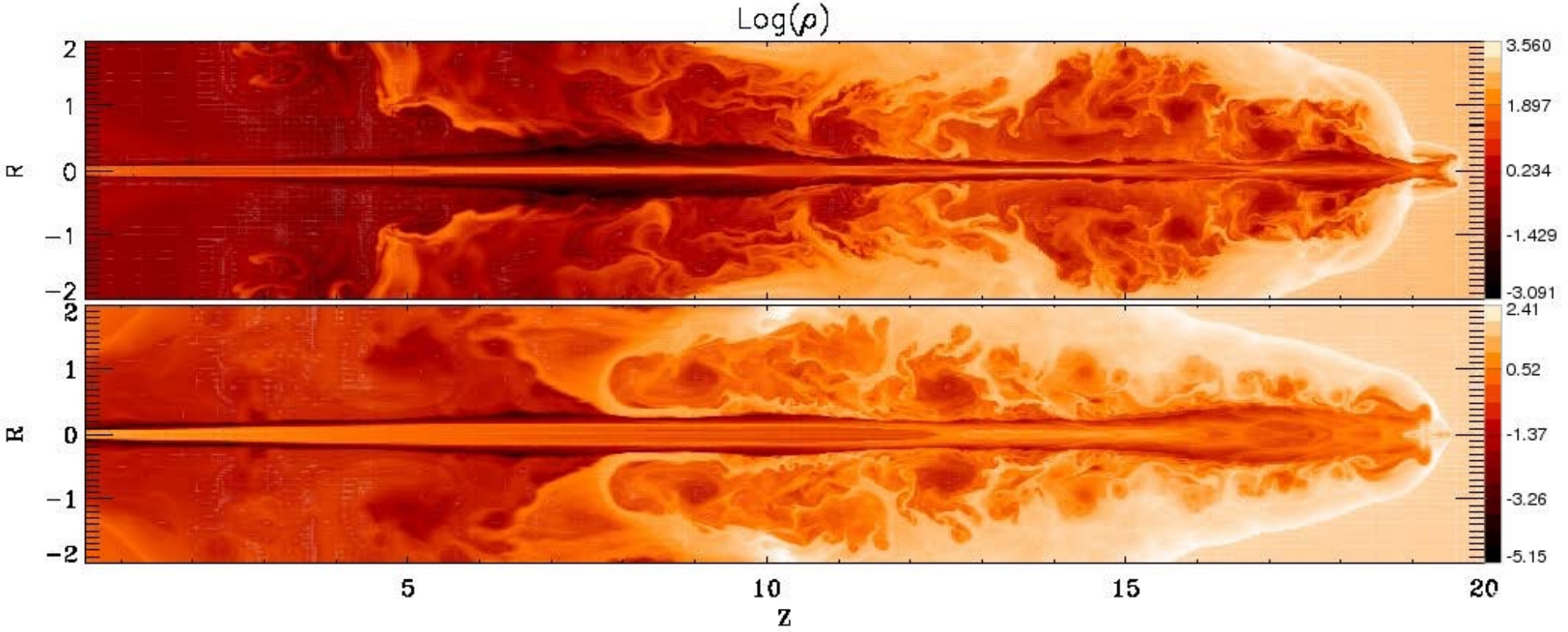

- Density structure in hydrodynamic simulations of relativistic jets, revealing nozzle formation, turbulent eddies and sheath-spine morphology.
- Meliani, Keppens & Giacomazzo, *Astron. & Astrophys.* **491**, 321 (2008)